Geochemistry Geophysics Geosystems G3

Article
Volume 12, Number 3
19 March 2011
Q03005, doi:10.1029/2010GC003355
ISSN: 1525-2027

Published by AGU and the Geochemical Society

Grain size control on Sr-Nd isotope provenance studies and impact on paleoclimate reconstructions: An example from deep-sea sediments offshore NW Africa

Inka Meyer
MARUM-Center for Marine Environmental Sciences, Leobener Straße, D-28359, Bremen, Germany (minka@marum.de)

Gareth R. Davies
Department of Petrology, Vrije Universiteit Amsterdam, De Boelelaan 1085, NL-1081 HV Amsterdam, Netherlands

Jan-Berend W. Stuut
MARUM-Center for Marine Environmental Sciences, Leobener Straße, D-28334, Bremen, Germany

NIOZ Royal Netherlands Institute for Sea Research, PO Box 59, NL-1790 AB Den Burg, Netherlands

[1] Five sediment cores from offshore NW Africa were analyzed for strontium and neodymium isotope ratios to reconstruct temporal variations in continental weathering regimes. Sediments were taken from three time slices with well-known and distinctive environmental conditions: present-day (dry and warm), ~6 ka (wet and warm), and ~12 ka (dry and cold). Terrigenous sediment samples were split into two size fractions to distinguish between the two dominant transport mechanisms offshore NW Africa: fluvial (0–10 μm) and aeolian (10–40 μm). Sr isotope data record evidence of marked grain size control with higher isotopic ratios in the fine fraction. In contrast, ε_{Nd} values are largely unaffected by grain size. Minor variability in Nd isotope data at each sampling site indicates near constant sources of terrigenous matter over the last ~12 ka. Variations in Sr isotope ratios are interpreted to reflect major changes in the evaporation-precipitation balance. We suggest that the Sr-Nd isotope data record a latitudinal shift of the northern limit of the African rainbelt and associated wind systems causing changes in the humidity and rate of chemical weathering over NW Africa. While hyperarid conditions prevailed ~12 ka, more humid conditions and intensified monsoonal rainfall at ~6 ka resulted in greater breakdown of easily weathered K-bearing phases and increased $^{87}Sr/^{86}Sr$ in the detritus. In late Holocene times the monsoonal circulation diminished resulting in a return to arid conditions. Our results clearly show that it is of vital importance in paleoenvironmental studies to carry out isotopic analyses on individual sediment fractions that were carried to the studied deposition site by distinct sediment transport mechanisms. If isotopic analyses are carried out on bulk sediments, the observed variability in isotopic values most likely represents changes in the particle size and mixing proportions of the sediment subpopulations.

Components: 8400 words, 5 figures, 1 table.

Keywords: Holocene; Sr-Nd isotopes; provenance; grain size effect.

Index Terms: 4914 Paleoceanography: Continental climate records; 1040 Geochemistry: Radiogenic isotope geochemistry; 3344 Atmospheric Processes: Paleoclimatology (0473, 4900).

Received 7 September 2010; **Revised** 10 January 2011; **Accepted** 3 February 2011; **Published** 19 March 2011.

Meyer, I., G. R. Davies, and J.-B. W. Stuut (2011), Grain size control on Sr-Nd isotope provenance studies and impact on paleoclimate reconstructions: An example from deep-sea sediments offshore NW Africa, *Geochem. Geophys. Geosyst.*, *12*, Q03005, doi:10.1029/2010GC003355.

1. Introduction

1.1. Provenance Studies

[2] The terrigenous fraction deposited in marine sediments offshore NW Africa forms an excellent archive of hydrological and climatic changes on the continent at different temporal and spatial scales [*Sarnthein et al.*, 1982; *Tjallingii et al.*, 2008]. In regions downwind of deserts, such as the Sahara, aeolian dust is the major component of the terrigenous fraction in deep-sea sediments [e.g., *Sarnthein et al.*, 1982]. Using satellite images, like Total Ozone Mapping Spectrophotometer (TOMS; Figure 1), the huge plume transporting dust from the African interior to the Atlantic can be easily monitored. The particle size of the transported dust varies as a function of the distance from source to sink and altitude at which the particles are transported [*Stuut et al.*, 2005]. Proximal aeolian dust from the Cape Verde Islands contain grains up to 90 μm in diameter [*Glaccum and Prospero*, 1980]. *Stuut et al.* [2005] detected particle sizes larger than 10 μm in modern atmospheric dust samples collected off Senegal and Mauritania. Although NW Africa is presently a dry region, terrigenous material supplied by rivers is another significant component in NE Atlantic sediments [*Holz et al.*, 2007]. Terrigenous material transported by rivers is much finer in size compared to the dust fraction. *Gac and Kane* [1986] investigated the fluvial sediment supplied by the Senegal River and found that 95% of the particles are smaller than 10 μm. Similar values were observed offshore of the Souss River system, which drains the Atlas Mountains in Morocco [*Weltje and Prins*, 2007].

[3] Grain size measurements can successfully distinguish between the different transport mechanisms of terrigenous sediments because the sediment-transport process leaves a characteristic grain size signature on the sediments it carries [e.g., *Stuut et al.*, 2002; *Weltje and Prins*, 2007]. Downcore measurements of grain sizes in marine sediment cores offshore NW Africa demonstrate a temporal change in the amount of fluvial and aeolian input, with an increase of fluvial supply during humid periods [e.g., *Tjallingii et al.*, 2008]. Conversely, during arid periods the amount of windblown material is higher than the fluvial supply [e.g., *Mulitza et al.*, 2008].

[4] Although grain size measurements can constrain different transport mechanisms, they are unlikely to be diagnostic of the geological source area of the terrigenous material or to reflect the environmental conditions on land. The aim of this study is to reconstruct the provenance of the terrigenous fraction and to investigate the hydrological changes in NW Africa since ~12 ka in three key time slices that represent known periods of extreme climate: present-day (dry and warm), mid-Holocene (wet and warm), and Younger Dryas (~12 ka, dry and cold). Therefore, in addition to grain size distributions of the terrigenous sediment fraction we report the strontium (Sr) and neodymium (Nd) isotopic composition of the terrigenous sediments to provide information on sediment provenance and continental weathering.

[5] Strontium is very mobile during chemical weathering and can be easily removed from the source region [*Blum and Erel*, 2003, 1997]. Therefore, variations in the $^{87}Sr/^{86}Sr$ ratio of sediments have been demonstrated to be a powerful tool to identify changes in the continental hydrology and chemical weathering regimes [e.g., *Blum and Erel*, 2003; *Jung et al.*, 2004; *Weldeab et al.*, 2002]. Contrary, Nd isotopes are not altered and therefore not fractionated during near-surface processes, such as chemical weathering. Hence, the isotopic composition of $^{143}Nd/^{144}Nd$ has been demonstrated to be a reliable indicator of the provenance of the terrigenous fraction of marine sediments [*Blum and Erel*, 2003; *Fagel et al.*, 2002; *Goldstein and O'Nions*, 1981].

[6] Consequently, combined Sr-Nd isotope analysis of sediments characterized by size-selective sediment-transport mechanisms potentially enables the distinction and quantification of the contribution of different source areas and the reconstruction of regional weathering regimes. This study applies this methodology to Holocene sediments offshore NW Africa to determine how the sedimentary record responds to major climatic changes.

1.2. Modern and Holocene NW African Climate

[7] Presently, two main features control the rainfall over NW Africa. In the southern parts of the Saharan Desert the West African monsoon generates

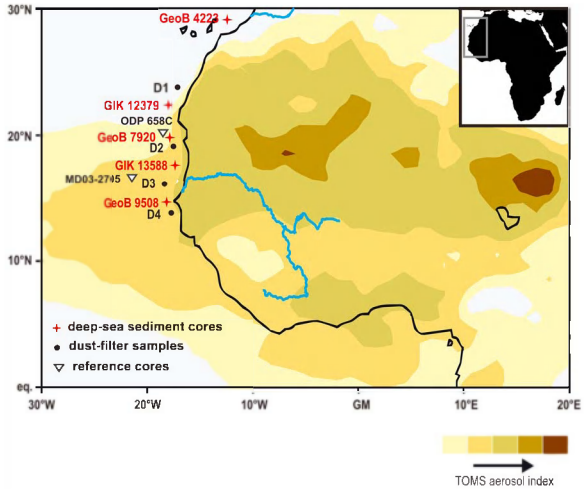

Figure 1. Averaged aerosol concentrations using TOMS (http://toms.gsfc.nasa.gov/) with location of sediment cores and averaged dust filter samples, labeled D1 to D4 (plotted is the middle position between start and end of sampling). White triangles display location of reference cores.

summer rainfall. The northern part is dominated by the migration of cyclones, causing winter rain [*Nicholson*, 2000]. The main driver of the atmospheric circulation over the region is the seasonal migration of the tropical rainbelt; its core lies at 5°N during boreal winter and at 19°N during boreal summer [*Nicholson*, 2000]. Besides these seasonal fluctuations it is assumed that the latitudinal position and/or the intensity of the wind belts has changed over geological time scales and caused variations in the hydrological conditions on land. Evidence for a change in the evaporation-precipitation balance in NW Africa during the Holocene is reported in several studies [e.g., *Gasse and van Campo*, 1994; *Gasse et al.*, 1990].

[8] The warming trend at the end of the Pleistocene is marked by a pronounced cold and dry period, the Younger Dryas, which is defined as a northern hemisphere event (YD; ~12.8 to 11.5 ka) [*Kennett*, 1990]. Evidence of the YD in NW Africa is widespread [*Gasse and van Campo*, 1994; *Marret and Turon*, 1994]. Proxy and model based reconstructions indicate a change in the atmospheric circulation and stronger northeastern trade winds as well as a shift to cooler and drier conditions throughout NW Africa [*Holz et al.*, 2007; *Marret and Turon*, 1994].

[9] After the termination of the YD, increased summer insolation and an intensified monsoon circulation linked to a northward shift of the African rainbelt over NW Africa caused more humid conditions and increased vegetation cover [*Nicholson et al.*, 1980; *Nicholson*, 2000; *Tjallingii et al.*, 2008]. Evidence for wetter conditions during the early and mid-Holocene was found in numerous geological, palynological, and hydrological records throughout NW Africa; the so-called African Humid Period (AHP) [e.g., *deMenocal et al.*, 2000a]. Based on an atmospheric general circulation model, *Kutzbach and Street-Perrott* [1985] concluded that the precipitation over the Sahel at 9 ka was ~30% higher than today. *deMenocal et al.* [2000b] reported 47% less aeolian dust supply to the Atlantic during the AHP, providing further evidence of significant climate change.

[10] In marine sediment cores offshore West Africa an increase in dust deposits is recorded since 5.5 ka toward the end of the Holocene, pointing to drier conditions [*deMenocal et al.*, 2000a]. Several proxy investigations report evidence of an aridification since the mid-Holocene throughout the Sahara and the Sahel [*Gasse and van Campo*, 1994]. These proxy-based investigations are consistent with climate-modeling studies [*Renssen et al.*, 2006].

1.3. Grain Size Effect in Sr and Nd Isotopes

[11] The impact of grain size on the isotopic fractionation in sedimentary rocks is a known but often neglected problem. Many studies have established differences in the isotopic signature of different grain size fractions [e.g., *Blum and Erel*, 2003; *Dasch*, 1969]. While the influence of grain size on the isotopic composition of Sr is proven by numerous studies (e.g., see review by *Blum and Erel* [2003]), the effect of grain size on Nd isotope ratios is still a matter of debate. *Dasch* [1969] was the first to report increasing $^{87}Sr/^{86}Sr$ ratios with decreasing grain size and vice versa. In contrast, comprehensive studies of the isotopic composition of $^{143}Nd/^{144}Nd$ have shown that Nd is largely unaffected by grain size variations. *Goldstein et al.* [1984] found only slightly changes of about $\pm 0.3\varepsilon_{Nd}$ between different size fractions of fluvial sediments. Recently, *Feng et al.* [2011] analyzed Sr and Nd concentrations in seven distinct size fractions from Chinese loess and aeolian dust. They discovered that the isotopic ratio of Sr is strongly influenced by grain size but that there is no influence on Nd values.

[12] Most previous Sr-Nd isotope provenance studies concentrated on bulk samples or single size fractions [e.g., *Cole et al.*, 2009; *Jullien et al.*, 2007]. However, numerous proxy studies suggest that there are variable contributions of detritus to individual sediments from distinctly different grain size

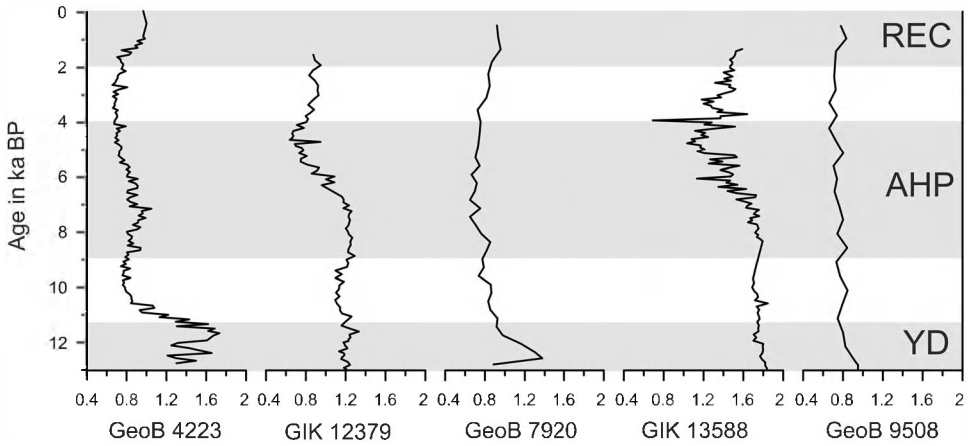

Figure 2. Log ratios of the median grain sizes of all five cores are calculated relative to a basis of 10 ($\log_{10}$) and plotted against sedimentary age. Grey bars are defined time slices of Recent times (REC), the African Humid Period (AHP), and Younger Dryas (YD).

fractions, related to different sediment-transport mechanisms, such as riverine suspension load and windblown dust [e.g., *Holz et al.*, 2007; *Stuut et al.*, 2002; *Weltje and Prins*, 2003]. Hence, different transport mechanisms contribute different grain size fractions, which should be visible in the isotopic composition as well. For a detailed paleoenvironmental interpretation or to reconstruct the evaporation-precipitation balance we need to take these grain size differences into account. The aim of this work is to quantify the magnitude of the grain size effect by using two different size fractions that represent clearly resolved end-members following detailed grain size analysis, a fine fraction (0–10 μm) and a coarse fraction (10–40 μm), representing fluvial mud, and aeolian dust, respectively.

2. Material and Methods

[13] This study was performed on five deep-sea sediment cores offshore NW Africa and sampled at three time slices, and four modern dust filter samples (Figure 1). The marine sediments (between 29°N and 15°N) and atmospheric dust samples were recovered during several cruises of R/V *Meteor* offshore Morocco, Western Sahara, Mauritania and Senegal. Exact locations of sediment cores and dust filter samples can be found in the auxiliary material.[1]

2.1. Grain Size Analyses

[14] In order to investigate variations in the sediment supply of the terrigenous fraction since the YD, grain size distributions were determined using a laser diffraction particle size analyzer (Beckman Coulter) LS200, resulting in 92 size classes from 0.4 to 2000 μm. Organic material, calcium carbonate, and biogenic silica were removed prior to measurements (see auxiliary material). To verify that all components were removed successfully, microscope analyses were carried out on selected samples. For the continuous Holocene grain size records, cores GeoB 4223, GIK 12379 and GIK 13588 were sampled every cm, core GeoB 9508 and GeoB 7920 every 5 cm. All pretreatments and grain size analyses were performed in the laboratories at MARUM, Bremen.

[15] Downcore $\log_{10}$ ratios of the median grain sizes of all cores are reported in Figure 2. To emphasize the trend, not amplitude, $\log_{10}$ ratios are chosen. As absolute dates were not always available for the individual sediment records, samples for isotope analyses were selected based on maxima and minima in the median grain size records, in combination with the published age models for the individual records (see auxiliary material). This means that samples were selected to cover the well-known climatic extremes (REC, recent; AHP, African Humid Period; YD, Younger Dryas) based on the observed expression of those extremes in the grain size data, rather than based solely on reconstructed age models. Generally, the YD yield coarsest grain sizes, while during the AHP finest grain sizes are observed. The REC period yields coarser material again. Grain size measurements of the dust filter samples show a mean grain size between 7.1 to 21.7 μm [*Stuut et al.*, 2005].

[1] Auxiliary materials are available in the HTML. doi:10.1029/2010GC003355.

Table 1. Results of Isotopic Measurements of All Five Deep-Sea Sediment Cores and Three Time Slices and the Four Dust Filter Samples[a]

Core	Period	Fraction	$^{143}Nd/^{144}Nd$ ($2\sigma \times 10^{-6}$)	ε_{Nd}	$^{87}Sr/^{86}Sr$ ($2\sigma \times 10^{-6}$)	Rb/ppm	Sr/ppm	$^{87}Rb/^{86}Sr$	Sm/ppm	Nd/ppm	$^{147}Sm/^{144}Nd$	T_{BE} (Ga)	T_{DM} (GA)	T_{BE}/T_{DM}
GeoB 4223	REC	0–10 μm	0.512058 (12)	−11.3	0.716003 (09)	133.0	283.4	1.359	8.20	45.02	0.11009	0.61	1.65	0.368
Duplicate					0.716771 (08)									
GeoB 4223	AHP	0–10 μm	0.512042 (12)	−11.6	0.713654 (07)	124.8	424.2	0.852	7.06	39.68	0.10754	0.80	1.64	0.485
Duplicate					0.713220 (10)									
GeoB 4223	YD	0–10 μm	0.512028 (12)	−11.9	0.712549 (12)	105.8	439.8	0.690	6.47	35.85	0.10908	0.87	1.68	0.518
Duplicate					0.711915 (09)									
GeoB 4223	REC	10–40 μm	0.512071 (14)	−11.0	0.716460 (09)	70.70	204.4	1.002	5.56	28.35	0.11854	0.88	1.89	0.460
Duplicate					0.716481 (10)									
GeoB 4223	AHP	10–40 μm	0.512053 (08)	−11.4	0.710725 (08)	53.58	537.5	0.289	5.28	26.11	0.12222	2.00	1.96	1.020
Duplicate					0.710688 (09)									
GeoB 4223	YD	10–40 μm	0.511993 (11)	−12.6	0.721564 (10)	16.23	51.13	0.927	0.35	1.85	0.11435	1.38	1.82	0.758
Duplicate					0.721557 (10)									
GIK 12379	REC	0–10 μm	0.511911 (09)	−14.2	0.725240 (08)	129.8	137.5	2.732	5.79	33.80	0.10354	0.54	1.75	0.307
GIK 12379	AHP	0–10 μm	0.511848 (14)	−15.4	0.725904 (14)	21.90	226.0	0.281	2.03	9.41	0.13038	0.52	1.74	0.297
GIK 12379	YD	0–10 μm	0.511910 (12)	−14.2	0.730458 (11)	101.6	82.82	3.550	5.22	30.87	0.10220	7.31	2.15	3.402
GIK 12379	REC	10–40 μm	–	–	0.718471 (10)	65.18	187.0	1.011	5.31	33.80	0.09495	1.02	–	–
GIK 12379	AHP	10–40 μm	–	–	0.720755 (23)	27.27	165.8	0.478	2.70	35.00	0.11615	2.80	–	–
GIK 12379	YD	10–40 μm	–	–	0.720560 (13)	28.35	38.11	2.170	0.20	30.87	0.09990	0.53	–	–
GeoB 7920	REC	0–10 μm	0.511876 (14)	−14.8	0.729342 (08)	58.90	68.57	2.509	2.95	17.40	0.10247	0.71	1.79	0.394
Duplicate					0.725364 (06)									
GeoB 7920	AHP	0–10 μm	0.511925 (09)	−13.9	0.723640 (08)	142.6	195.8	2.109	6.51	38.66	0.10177	0.65	1.71	0.378
Duplicate					0.721890 (09)									
GeoB 7920	YD	0–10 μm	0.511869 (10)	−15.0	0.729979 (10)	95.19	255.2	1.080	4.84	28.62	0.10221	0.36	1.62	0.219
Duplicate					0.729981 (07)									
GeoB 7920	REC	10–40 μm	0.511942 (08)	−13.5	0.718066 (09)	67.80	208.1	0.944	4.50	22.80	0.11929	1.07	1.99	0.537
Duplicate					0.717641 (06)									
GeoB 7920	AHP	10–40 μm	0.511843 (09)	−15.4	0.717148 (10)	24.61	91.25	0.780	1.93	8.95	0.13033	1.43	2.43	0.588
Duplicate					0.716607 (10)									
GeoB 7920	YD	10–40 μm	0.511795 (08)	−16.4	0.727354 (09)	28.60	45.66	1.830	0.52	3.16	0.09946	0.29	1.84	0.156
Duplicate					0.727332 (11)									
GIK 13588	REC	0–10 μm	0.511897 (10)	−14.4	0.725818 (13)	161.1	145.2	3.212	6.79	38.65	0.09336	0.47	1.63	0.287
GIK 13588	AHP	0–10 μm	0.511909 (10)	−14.2	0.720430 (18)	47.30	121.7	1.125	1.15	6.33	0.08815	1.04	1.65	0.672
GIK 13588	YD	0–10 μm	0.511932 (11)	−13.7	0.726690 (10)	140.5	151.1	2.690	7.41	33.35	0.09084	0.59	1.79	0.418
GIK 13588	REC	10–40 μm	–	–	0.718345 (09)	11.20	52.36	0.620	2.64	13.50	0.11819	1.75	–	–
GIK 13588	AHP	10–40 μm	–	–	0.718634 (09)	66.20	184.6	1.038	15.00	35.00	0.25904	0.56	–	–
GIK 13588	YD	10–40 μm	–	–	0.712188 (09)	24.81	23.35	3.154	0.30	1.45	0.12505	0.17	–	–
GeoB 9508	REC	0–10 μm	0.511920 (11)	−14.0	0.724864 (06)	43.90	58.13	2.188	2.47	14.32	0.10425	0.66	1.75	0.379
Duplicate					0.725033 (08)									
GeoB 9508	AHP	0–10 μm	0.511923 (09)	−13.9	0.721935 (07)	109.75	117.2	2.712	5.43	30.07	0.10700	0.22	1.64	0.136
Duplicate					0.721929 (09)									

Table 1. (continued)

Core	Period	Fraction	$^{143}Nd/^{144}Nd$ ($2\sigma \times 10^{-6}$)	ε_{Nd}	$^{87}Sr/^{86}Sr$ ($2\sigma \times 10^{-6}$)	Rb/ppm	Sr/ppm	$^{87}Rb/^{86}Sr$	Sm/ppm	Nd/ppm	$^{147}Sm/^{144}Nd$	T_{BE} (Ga)	T_{DM} (GA)	T_{BE}/T_{DM}
GeoB 9508	YD	0–10 μm	0.511918 (09)	−14.0	0.725970 (09)	65.16	147.4	1.286	5.48	30.48	0.10521	0.51	1.65	0.317
Duplicate					0.725177 (13)									
GeoB 9508	REC	10–40 μm	0.511875 (14)	−14.8	0.719875 (07)	35.50	112.94	0.847	2.36	12.24	0.10247	1.56	1.79	0.871
Duplicate					0.711541 (10)									
GeoB 9508	AHP	10–40 μm	0.511862(08)	−15.1	0.719413 (06)	68.10	156.4	1.173	4.46	22.51	0.10601	0.93	1.86	0.501
Duplicate					0.719830 (06)									
GeoB 9508	YD	10–40 μm	0.511890 (09)	−14.6	0.723053 (09)	25.38	73.43	0.942	3.04	14.87	0.10865	1.38	1.85	0.863
Duplicate					0.723478 (10)									
Dust Filter 1	REC	10–40 μm	0.511900 (10)	−14.3	0.719584 (14)									
Dust Filter 2	REC	10–40 μm	0.511881 (09)	−14.7	0.719579 (12)									
Dust Filter 3	REC	10–40 μm	0.511872 (09)	−14.9	0.723345 (09)									
Dust Filter 4	REC	10–40 μm	0.511908 (10)	−14.2	0.722852 (08)									

[a]Due to the limited sample size, Nd measurements of GIK 12379 and GIK 13588 are only available for the fine fraction. For Sr duplicates from a separate solution are listed.

[16] Based on published end-member modeling studies [*Holz et al.*, 2004; *Tjallingii et al.*, 2008] we separated our terrigenous fraction into two size classes. The fine fraction (0–10 μm) is interpreted as fluvial input, the coarse fraction (10–40 μm) as aeolian material. Grain size separation was undertaken in settling tubes using Stoke's Law. Grain size analyses of the single size fractions indicated only minor overlap between both fractions. Furthermore, differences in the mineralogy of the two size fractions were determined by visual inspection using a binocular microscope.

2.2. Sample Preparation

[17] Sample preparations for the isotopic analyses were carried out in a "class 100" clean laboratory at the VU Amsterdam. In order to dissolve all authigenic, biogenic carbonate, and absorbed marine Sr-Nd signals, all samples were leached with 1*N* HCl and the dissolved fraction discarded before digestion. Subsequently, samples were dissolved in a HF-HNO_3-HCl mixture. In order to dissolve any possible refractory phases such as zircon, dissolutions of the coarser fractions were performed in Teflonlined acid digestion bombs at 200°C for 5 days. Two international standards (BHVO-2, MAG-1) were also included in the analytical procedure. Values for standard BHVO-2 gave a value of 0.703488 ± 0.000007 (2σ; n = 5) for $^{87}Sr/^{86}Sr$ and 0.512987 ± 0.000005 (2σ; n = 3) for $^{143}Nd/^{144}Nd$. Standard MAG-1 gave a value of 0.722638 ± 0.000009 (2σ; n = 3) for $^{87}Sr/^{86}Sr$ and 0.512070 ± 0.000008 (2σ; n = 2) for $^{143}Nd/^{144}Nd$.

2.3. Isotope Analysis

[18] Isotopic measurements were performed at the VU Amsterdam. Strontium isotope compositions were determined using a MAT 262 Thermal Ionisation Mass Spectrometer (TIMS). Samples were loaded onto single rhenium filaments and measured in static mode. $^{87}Sr/^{86}Sr$ ratios were corrected for mass fractionation by normalizing to $^{86}Sr/^{88}Sr$ = 0.1194. Over the period of the study, the NBS 987 standard gave an average values of $^{87}Sr/^{86}Sr$ = 0.710241 ± 0.000004 (2σ; n = 10). Blanks typically yield < 200 pg so that blank contribution to the analyses can be neglected. Duplicate Sr isotope analyses were performed on separate solutions for some samples (Table 1). The results show that nearly all duplicates fall within uncertainty limits and variations have been considered negligible considering the overall variation of isotopic compositions.

[19] Neodymium isotope ratios were measured using a ThermoFinnigan Neptune MC-ICP-MS.

$^{143}Nd/^{144}Nd$ isotope ratios were corrected for mass fractionation by normalizing to $^{146}Nd/^{144}Nd$ = 0.7219. An internal standard, CIGO, is used to monitor the Neptune's performance. The analysis of CIGO gave an average value of $^{143}Nd/^{144}Nd$ = 0.511342 ± 0.000004 (2σ; n = 10), which equates to a value for the La Jolla international standard determined by TIMS of 0.511850 ± 0.000008 (n = 43). Isotope values for all samples are reported in Table 1. Results are reported as $^{143}Nd/^{144}Nd$ and as ε_{Nd} [$\varepsilon_{Nd} = (((^{143}Nd/^{144}Nd$ sample/0.512636)−1) × 10^4] using the present-day "chondritic uniform reservoir" (CHUR) value of 0.512636 [*Jacobsen and Wasserburg*, 1980]. An aliquot (~5%) of each sediment size fraction was analyzed for trace elements concentrations using a Quadrupole Thermo X-Series II ICP-MS.

3. Results

[20] Measured Nd isotope ratios range between ε_{Nd} −11.0 and −16.4 (Table 1). There is a clear difference between the northernmost core (−11.0 to −12.6) and the four cores retrieved between 23°5 S and 15°5 S (−13.5 to −16.4). Differences in Nd isotope ratios between the three periods in each core are relatively small in all cores. In contrast, $^{87}Sr/^{86}Sr$ ratios vary significantly, between 0.7172 and 0.7304 (Table 1). Data for the fine fraction range between 0.7160 and 0.7293 in the REC. Compared to the REC fine fraction, the $^{87}Sr/^{86}Sr$ ratios of the fine fraction of the AHP time slice are less radiogenic, between 0.7136 and 0.7259. $^{87}Sr/^{86}Sr$ ratios for the fine fraction of the YD are between 0.7126 and 0.7305, reaching values higher than for the REC period. A similar relationship can be observed in the 10–40 μm fractions, where REC samples range between 0.7164 and 0.7199. AHP samples are less radiogenic (0.7107 to 0.7207). The YD has more radiogenic values than the REC, with ratios between 0.7122 and 0.7274. The Sr isotope ratios of the coarse REC samples are within the range recorded for the dust filter samples (0.7196 to 0.7233) and confirm that the terrigenous sediment fractions contain a good archive of detritus eroded from NW Africa.

[21] In order to estimate the temporal geochemical evolution of the source regions, Nd and Sr isotope data were used to calculate model ages of the terrigenous material relative to depleted mantle (T_{DM}) and Bulk Earth (T_{BE}; Table 1). The majority of Nd and Sr model ages vary between 1.62 and 2.43 Ga and 0.22–2.80 Ga, respectively. The T_{BE} value of 7.31 Ga, calculated for the fine fraction of the YD in core GIK 12379, is considered as an outlier and is not taken into account for further discussion. T_{DM} model ages are generally older in the coarse fraction than in the fine fraction. Highest Nd model ages are found in the AHP coarse fraction. Importantly, there is no significant difference between T_{DM} ages of the fine fractions. The Rb/Sr ratio of continental crust is increased by several intracrustal processes, for example crustal melting or weathering. The greater the number of times crustal material is subjected to such processes the greater the increase in the Rb/Sr ratio [*Blum and Erel*, 2003; *McDermott and Hawkesworth*, 1990]. In contrast, REE abundances are hardly changed by intercrustal processes so that Sm/Nd remains relatively constant in the upper crust [*Blum and Erel*, 2003]. The effect of increasing Rb/Sr is that Sr model ages (T_{BE}) are reduced whereas Nd model ages (T_{DM}) remain hardly changed. A monitor of the changes caused to Rb/Sr by variations of physical and chemical weathering in sedimentary source regions is therefore provided by the ratio of Sr and Nd model ages; T_{BE}/T_{DM} (see Table 1) [*Davies et al.*, 1989; *McDermott and Hawkesworth*, 1990]. This ratio averages 0.35 for the fine fraction compared to 0.63 for the coarse fraction.

4. Discussion

4.1. Grain Size Effect

[22] We analyzed Sr and Nd in two separate grain size fractions in order to identify if there is a grain size effect on the isotopic composition of both elements. Our measurements confirm that the grain size effect on the Sr isotope composition is significant and must be taken into account when Sr isotope values are interpreted in terms of provenance and/or weathering intensity. It is apparent from Figure 3 that $^{87}Sr/^{86}Sr$ ratios vary as a function of grain size independently of any climatic fluctuations (Figure 3, left). Thirteen of fifteen samples of the fine fraction (open symbols) display higher $^{87}Sr/^{86}Sr$ isotopic ratios than the coarse fraction (filled symbols). This isotopic variation is most obvious within the AHP (Figure 3, middle). The fine fraction has an average ratio of ~0.721 ± 0.000011 (2σ, n = 5), whereas the coarse fraction yields ~0.716 ± 0.000011 (2σ, n = 5). A similar difference is also recorded by the REC samples, where the average ratio of the fine fraction is ~0.724 (2σ, n = 5) and ~0.718 (2σ, n = 5) in the coarse fraction, as well as in the YD samples, with ~0.725 (2σ, n = 5) in the fine fraction and

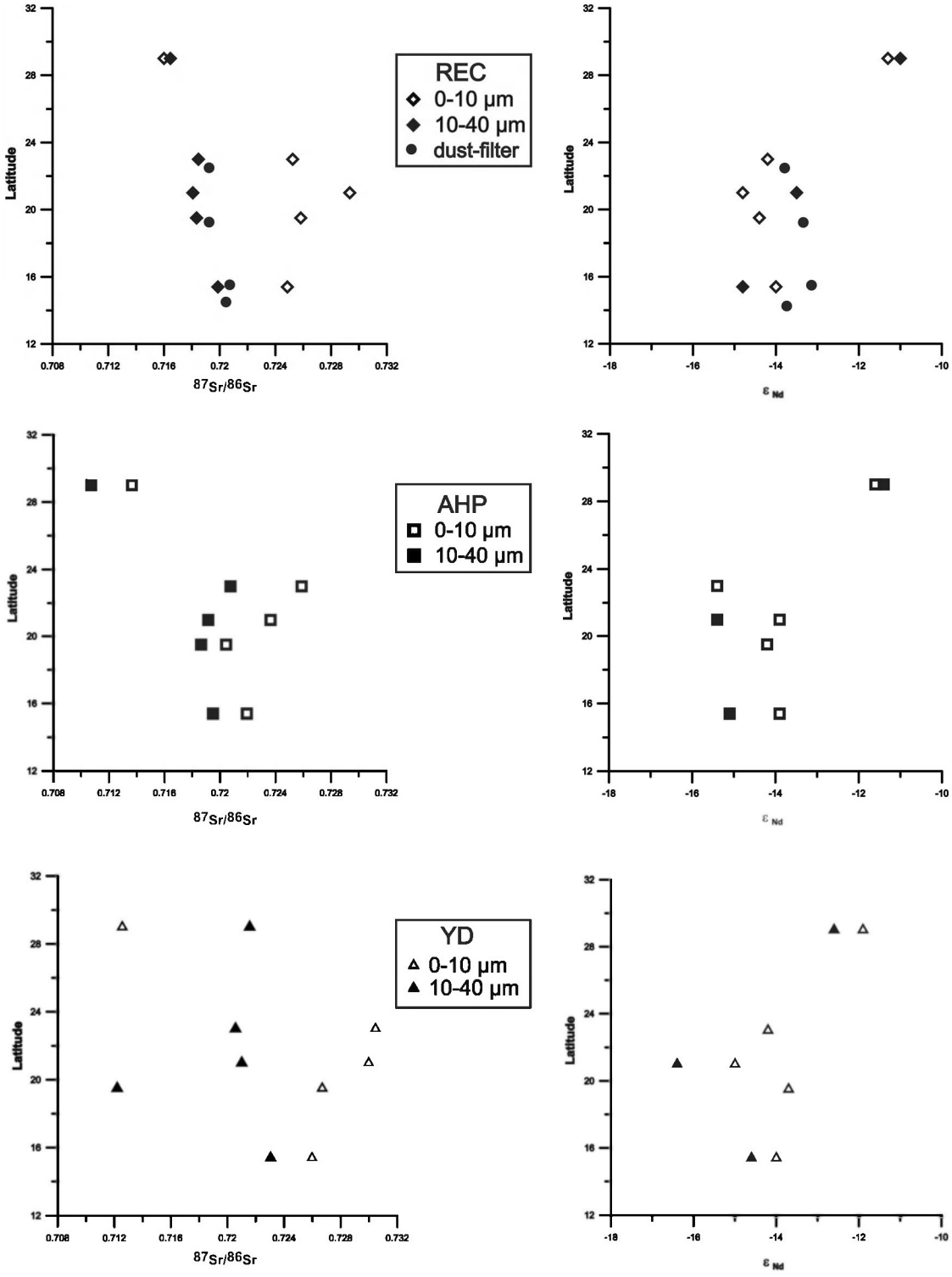

Figure 3. Isotopic variations of (left) Sr and (right) Nd with grain size. Figure 3 clearly demonstrates that Sr isotopes are strongly influenced by grain size. The fine fraction (open symbols) shows generally more radiogenic values than the coarse fraction (filled symbols). Nd isotopes are not influenced by grain size.

~0.721 (2σ, n = 5) in the coarse fraction. Hence, our $^{87}Sr/^{86}Sr$ data demonstrate that there is a significant contrast between the fine and coarse size fractions. Isotopic measurements on bulk sediment samples that are not split into size fractions would give a mixed signal of both size fractions. If transport processes lead to variations in the input of the different size fractions, then bulk analyses will give biases in the isotopic measurements.

[23] One possible reason for the grain size effect could be found in the mineralogy of the samples. From the visual inspection of the samples we know that the coarse fraction is dominated by quartz and feldspar while the fine fraction is enriched in clay minerals and micas. Our observation is corroborated by other investigations of Saharan dust and fluvial supply [*Pye*, 1987; *Stuut et al.*, 2005]. Since Sr is produced by the radioactive decay of Rb, sediments derived from Rb-bearing phases such as clay minerals, yield high $^{87}Sr/^{86}Sr$ rations [*Blum and Erel*, 1997]. However, minerals exhibit different response to chemical weathering [*Blum and Erel*, 1997], with quartz showing a strong resistance to chemical weathering whereas feldspars and clays are more easily broken down. Since Sr is more readily released into solution than Rb during chemical weathering, finer-grained weathering products tend to be enriched in Rb-bearing alteration products such as clays [*Blum and Erel*, 1997; *Faure*, 1986]. Therefore, during enhanced chemical weathering, particles and minerals become smaller in size and Sr isotope ratio increases with decreasing particle size. In summary, strontium isotope ratios in sediments are generally higher than the parent rocks and this tendency is more extreme with smaller sediment grain sizes, and with higher influence of chemical weathering. In terms of Sr isotope ratios, quartz acts almost as an inert phase in sedimentary systems diluting the influence of Rb- and Sr-bearing phases. The data presented in this study demonstrate that grain size has a significant impact on the isotopic composition of Sr. Consequently, investigations of bulk sediment samples without grain size separations are hard to interpret as the observed changes in isotopic values could simply be the result of changes in grain size due to varying input of dust and fluvial material. Therefore, great care should be taken with the interpretation of analyses in which size separation has not been performed.

[24] In contrast, ε_{Nd} appears unaffected by grain size (Figure 3, right). Averaged ε_{Nd} values for the coarse and fine fractions are very similar, with −13.4 in the fine fraction and −13.8 in the coarse fraction. Equally, the Nd isotope difference between fine and coarse fractions within the different time periods is also minor; REC is 0.3 ε_{Nd}, for the AHP 0.8 ε_{Nd} and for the YD 0.9 ε_{Nd}. Our data support the findings of *Goldstein et al.* [1984] that grain size has no significant effect on the ε_{Nd} composition. However, in all cases calculated T_{DM} model ages are older in the coarse than the fine fraction. Since there is no change in the ε_{Nd} values between the fine and the coarse fractions, the difference in model ages can only be due to higher Sm/Nd ratios in the coarser fractions due to variations in the mineralogy of the samples or to greater abundance of heavy minerals such as zircon [*White et al.*, 1986].

4.2. Provenance of Marine Sediments off NW Africa

[25] The Nd isotope composition of marine sediments can be influenced by the isotopic composition and crustal age of their parent rocks and by mixing with other material during transport between source and sink. Since Nd isotopes are not fractionated by chemical weathering we use ε_{Nd} as a tracer of the geological provenance. The isotopic data show a clear difference between the northern core off Morocco (~−11.6 ε_{Nd}) and the cores off Mauritania and Senegal (between −13.5 and −16.4 ε_{Nd}). The observed ε_{Nd} values can be explained by the diverse geology in the area (Figure 4). Most of the NW African basement belongs to the West African Craton extending from the Atlas Mountains in the north to the Gulf of Guinea in the south. The Craton is mainly made up of late Archaean and early mid Proterozoic crystalline basement rocks (~2.0 Ga) [*Lecorche et al.*, 1991]. The oldest rocks are 3.5–3.6 Ga and are exposed in the southwestern part of the Reguibat shield (Figure 4) [*Potrel et al.*, 1996]. The Craton is bounded by the Atlas Mountains in the NNW which were formed much later in several phases of Earth's history [e.g., *Ennih and Liegeois*, 2008]. The last period of tectonic deformation occurred during the Late Cretaceous–Cenozoic (~65 Ma) when Africa and Eurasia started colliding [*Wright et al.*, 1985]. Therefore, the more radiogenic ratios of GeoB 4223 off Morocco are a consequence of the younger material eroded from the Atlas Mountains. T_{DM} model ages given in Table 1 demonstrate that core GeoB 4223 yields T_{DM} ages of ~1.66 Ga in the fine fraction and ~1.83 Ga in the coarse fraction. In contrast T_{DM} model ages for the southern cores are older, with ~1.74 Ga in the fine and ~1.96 Ga in the coarse fraction. We interpret the isotopic values of the southern cores as dominated by the Archaean West African Craton.

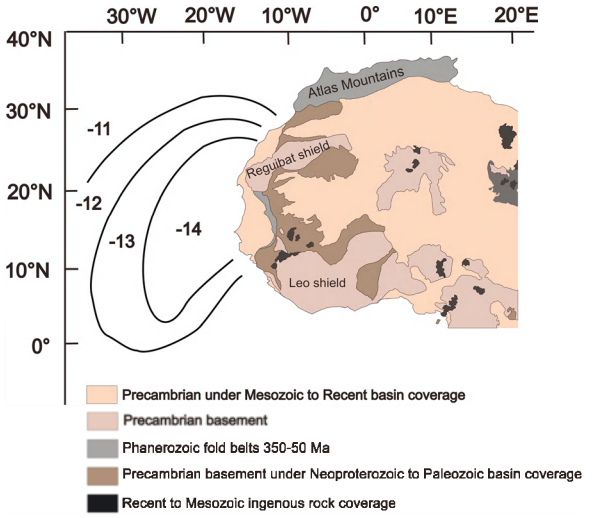

Figure 4. Geological map of NW Africa (modified from *Trauth and Schlüter* [2006]). Map shows the present-day ε_{Nd} distributions of surface sediments (modified from *Grousset et al.* [1998]).

[26] On a Sr-Nd mixing diagram (Figure 5) we interpret the mixtures of the investigated sediments between two possible end-members of the terrigenous fraction proposed by *Grousset et al.* [1998]. In agreement with these data the samples presented in this study allow a distinction between the relatively unradiogenic northerly sediment, influenced by sources in the Atlas Mountains, and a southerly source dominated by the very unradiogenic signal derived from the Archaean outcrops in Mauritania with ε_{Nd} values between −20.4 and −54.2 [*Potrel et al.*, 1996]. The ε_{Nd} variability in the source areas is, however, not reflected by any resolvable temporal variation in the individual cores sampled in the eastern Atlantic Ocean. This observation implies that the provenance of the sediment has remained constant over the entire Holocene.

[27] Similar findings were recently reported by *Cole et al.* [2009]. They studied marine sediment core ODP 658C offshore Mauritania (Figure 1) where they found only minor variability of < 0.9 ε_{Nd} throughout the last 25 ka. Further support for a constant sediment provenance comes from the work of *Jullien et al.* [2007] who analyzed marine sediment core MD03–2705 offshore Mauritania (Figure 1). They found no difference in ε_{Nd} values between the YD (−14.6) and glacial sediments (−14.7). Furthermore, *Grousset et al.* [1998] studied < 30 μm sediment fractions from the Recent and the Last Glacial Maximum (LGM) offshore NW Africa and reported no significant changes in ε_{Nd} values between the surface samples and the LGM samples.

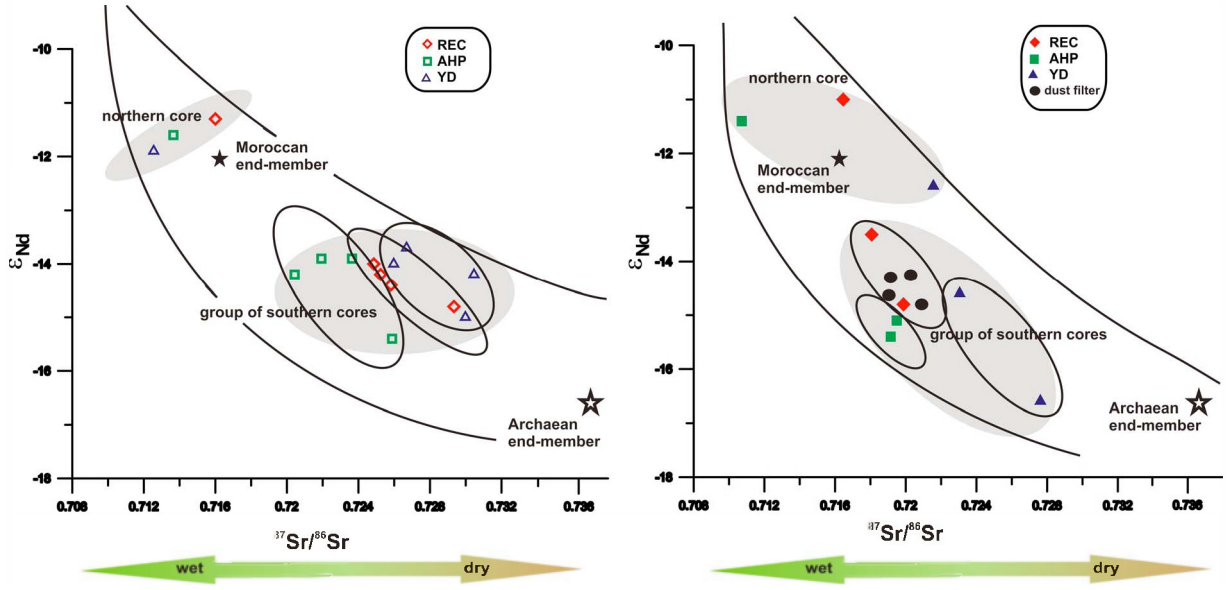

Figure 5. A comparison between the isotopic compositions of $^{87}Sr/^{86}Sr$ and ε_{Nd} for (left) the fine and (right) the coarse fraction. Figure 5 shows the distinctions between the three periods (ellipse). During the YD (triangles) hyperarid conditions are prevailing, and during the AHP (squares) moist conditions can be observed. At recent times (diamonds) a return to dry conditions is indicated. Present-day dust filter samples (dots; obtained from *Stuut et al.* [2005]) are in line with REC samples. The ε_{Nd} dates show a clear difference of the geologic source area between the northern core and the group of cores south of 23°N. A comparison between both size fractions shows the same trend but a different isotopic ratio. To define possible end-members, data from dust source regions on land are included [see *Grousset et al.*, 1998].

Therefore, they proposed no significant change in the source area of sediments between the LGM and modern times.

[28] To summarize, the variability in the ε_{Nd} values of sediment size fractions from NW Africa indicates that there are two major source areas. The northern core is influenced by the younger and more radiogenic material originating from the Atlas Mountains and a more southern source dominated by the very unradiogenic old basement rocks of the West African Craton. The minimal changes in the isotopic records suggest changes in the intensity of the different source areas but no major change in the geological source area since the YD.

4.3. Changes in Chemical Weathering Regime During the Holocene

[29] In marked contrast to the minor changes recorded by ε_{Nd} values, $^{87}Sr/^{86}Sr$ ratios document large variations within the different sediment cores (between 0.7107 and 0.7305). Since our study was performed on distinct grain size fractions we minimized the influence of any grain size or mineralogical control. In addition, the size separation allows the distinction between aeolian dust (10–40 μm) and fluvial input (0–10 μm). During times of enhanced chemical weathering more ^{87}Sr is eluted from the source material [*Blum and Erel*, 2003]. Hence, low Sr isotopic ratios are interpreted to reflect an increase in chemical weathering and vice versa; during arid conditions the effect of chemical weathering is diminished and the Sr isotopic ratio is generally higher [*Blum and Erel*, 1997, 2003; *Jung et al.*, 2004]. Thus, corroborating with previous studies, we interpret the observed variations in $^{87}Sr/^{86}Sr$ as predominantly a consequence of changes in the evaporation-precipitation balance and the amount of chemical weathering [e.g., *Åberg et al.*, 1989; *Blum et al.*, 1993; *Blum and Erel*, 1997, 2003; *Capo et al.*, 1998; *Dasch*, 1969; *Derry and France-Lanord*, 1996; *Jung et al.*, 2004]. The temporal variations in the isotopic record are illustrated in Figures 3 and 5. Since the evaporation-precipitation balance and hence the humidity over NW Africa is mainly influenced by the African rainbelt [e.g., *Mulitza et al.*, 2008], our data can be used as a proxy for latitudinal movements of this rainbelt during the last 12 ka. Fine fraction samples offshore Mauritania and Senegal have the highest $^{87}Sr/^{86}Sr$ ratios (~0.725) during the YD implying dry, desert-like conditions. Samples from the AHP are lower (~0.717), indicating increased humidity and enhanced chemical weathering. $^{87}Sr/^{86}Sr$ ratios of the REC fine fraction (~0.729) display a return to the modern arid conditions within the Sahara region. Similar temporal changes are observed in the coarse fraction. Sr isotope ratios of the coarse REC fraction are comparable to the dust filter samples (~0.721; Table 1) and these data indicate that the recent sediments represent a true proxy of material eroded from NW Africa under modern dry conditions.

[30] The fine sediment fractions of core GeoB 4223 record a different relationship compared to the southern cores, with lower $^{87}Sr/^{86}Sr$ values (0.7126), indicating wettest conditions during the YD. A higher $^{87}Sr/^{86}Sr$ ratio during the AHP (0.7137) suggests drier conditions during the AHP than within the YD. In recent times, the fine fraction from the northern core is consistent with the current arid conditions in having the most radiogenic Sr isotope ratio of the three time intervals (0.7160). The coarse fraction of GeoB 4223 has a different signal compared to the fine fraction. The $^{87}Sr/^{86}Sr$ values record comparable variations to the southern cores, with driest conditions during the YD (~0.721), wetter conditions during the AHP (~0.710) and a return to drier conditions in modern times (~0.716). Due to the complex isotopic variations recorded in the different fractions of core GeoB 4223, we propose that during the YD there was a seasonal influence of extratropical cool and humid west wind systems.

[31] Variations in the atmospheric circulation over NW Africa and/or a shift in the latitudinal position of the African rain belt are indicated by several studies [e.g., *Liu et al.*, 2007]. Potentially, the northern front of the monsoon belt moved about 700 km to the north during the AHP. The opposite movement is implied during glacial times when the African rainbelt shifted equatorward compared to modern times [*Hooghiemstra*, 1988]. As a consequence, the northernmost part of North Africa was influenced by the North Atlantic climate system. Measured Sr isotope ratios of the fine fraction of core GeoB 4223 are in agreement with this finding, they indicate most humid conditions during the YD. During the AHP the African rainbelt had a more northern position than today. While the general climate of NW Africa was more humid during the AHP, the northern part of the African continent was generally wet, but outside the influence of the extratropical wind systems [*Nicholson*, 2000]. Hence, Sr isotope ratios of the northern core indicate drier conditions during the AHP than during the YD. A northward shift or an expansion of the African rainbelt and the monsoon winds

during the mid-Holocene explain the opposing climatic trends indicated by the northern and southern cores.

[32] A more quantitative way of examining the effect of weathering processes on the different size fractions is to calculate ratios between T_{BE} and T_{DM} (Table 1). Given that REE fractionation by weathering processes is minimal [e.g., *Blum and Erel*, 2003], the T_{BE}/T_{DM} ratio is mainly dominated by fractionation in Rb/Sr [e.g., *Davies et al.*, 1985; *McDermott and Hawkesworth*, 1990]. During times of enhanced chemical weathering associated with a wetter environment more ^{87}Sr is released into solution from the source rocks due to the preferential breakdown of Rb-rich phases such as mica and K-feldspar. This leads to a greater fractionation of Rb-Sr isotope during more humid periods and to a lower T_{BE}/T_{DM} ratio in the sediments produced. Such systematic can be observed in core GeoB 9508 where T_{BE} ages are lowest during the AHP period for both size fractions. Additionally, the lowest T_{BE}/T_{DM} ratios are found in the AHP period for fine and coarse fractions. Calculated T_{BE}/T_{DM} ratios for the other four cores do not show such consistency. T_{BE}/T_{DM} ratios are higher during the AHP than during the REC and YD in the coarse fraction. Within the fine fraction no clear temporal variations can be resolved. This observation suggests that the combination of grain size control of Rb/Sr and different aeolian and fluvial inputs does not always yield coherent behavior in the Rb-Sr system. Core GeoB 9508 with the coherent variations in T_{BE}/T_{DM} is located in the vicinity of the Senegal River. The generally humid environment at this latitude and the continuous supply of fluvial matter would be expected to cause a lower T_{BE}/T_{DM} ratio due to a greater abundance of Rb-rich phases in the fluvial material. In contrast, the other cores record more complex Sr and Nd isotope systematics most likely influenced by variations in the input of aeolian and fluvial material.

5. Conclusions

[33] The Sr-Nd isotope records from different marine sediment cores along the NW African coast are used to document a detailed provenance and weathering record in three time slices since the YD. Nd isotope ratios record minimal changes over time, indicating little change in the provenance of the different source materials and no significant change in the geological source area since the YD. By contrast, major variations in Sr isotope ratios indicate large changes in the humidity and rate of chemical weathering during the Holocene. The combined Sr-Nd isotope data indicate a latitudinal shift or an expansion of the African rainbelt and the associated wind belts causing changes in the evaporation-precipitation balance over NW Africa. While hyperarid conditions prevail during the YD, more humid conditions and intensified monsoonal rainfall characterize the AHP. In late Holocene times the monsoonal circulation diminished causing a return to arid conditions in NW Africa. In addition, our data clearly demonstrate that the isotopic ratio of $^{87}Sr/^{86}Sr$ is strongly influenced by grain size and that the isotopic ratio is generally higher in the fine fraction. As a result, investigations of bulk sediment samples without grain size separations are hard to interpret. We recommend that grain size separation is utilized in all studies of the geochemical and isotopic variations in detrital sediments. A further detailed investigation incorporating grain size measurements and isotope analyses on mineralogically well-constrained sediments is required to improve our understanding of the influence of variations in the amount of dust and fluvial matter on the isotopic fractionation.

Acknowledgments

[34] We thank Bas van der Wagt for measuring Nd samples on the Neptune and for ICP-MS measurements. Martijn Klaver is thanked for providing help with TIMS measurements. We thank Richard Smeets for all the help in the clean lab and with chemical procedures. We thank Natalie Fagel and an anonymous reviewer for critical reviews and constructive comments. This research was funded by the Deutsche Forschungsgemeinschaft (DFG) through the European Graduate College EUROPROX and MARUM-Center for Marine Environmental Sciences, with additional funding from Europlanet.

References

Åberg, G., et al. (1989), Weathering rates and $^{87}Sr/^{86}Sr$ ratios: An isotopic approach, *J. Hydrol.*, *109*(1–2), 65–78, doi:10.1016/0022-1694(89)90007-3.

Blum, J. D., and Y. Erel (1997), Rb-Sr isotope systematics of granitic soil chronosequence: The importance of biotite weathering, *Geochim. Cosmochim. Acta*, *61*(15), 3193–3204, doi:10.1016/S0016-7037(97)00148-8.

Blum, J. D., and Y. Erel (2003), Radiogenic isotopes in weathering and hydrology, in *Surface and Ground Water, Weathering, and Soils, Treatise Geochem.*, vol. 5, edited by J. I. Drever, pp. 365–369, Elsevier, Oxford, U. K.

Blum, J. D., et al. (1993), $^{87}Sr/^{86}Sr$ ratios of sierra nevada stream waters: Implications for relative mineral weathering rates, *Geochim. Cosmochim. Acta*, *57*(21–22), 5019–5025, doi:10.1016/S0016-7037(05)80014-6.

Capo, R. C., et al. (1998), Strontium isotopes as tracers of ecosystem processes: Theory and methods, *Geoderma*, *82*(1–3), 197–225, doi:10.1016/S0016-7061(97)00102-X.

Cole, J. M., et al. (2009), Contrasting compositions of Saharan dust in the eastern Atlantic Ocean during the last deglaciation and African Humid Period, *Earth Planet. Sci. Lett.*, *278*(3–4), 257–266, doi:10.1016/j.epsl.2008.12.011.

Dasch, E. J. (1969), Strontium isotopes in weathering profiles, deep-sea sediments, and sedimentary rocks, *Geochim. Cosmochim. Acta*, *33*(12), 1521–1552, doi:10.1016/0016-7037(69)90153-7.

Davies, G. R., et al. (1985), Upper crustal recycling in southern Britain: Evidence from Nd and Sr isotopes, *Earth Planet. Sci. Lett.*, *75*(1), 1–12, doi:10.1016/0012-821X(85)90045-7.

Davies, G. R., R. A. Cliff, M. J. Norry, and D. C. Gerlach (1989), A combined chemical and Pb-Sr-Nd isotope study of the Azores and Cape Verde hot-spots: The geodynamic implications, in *Magmatism in the Ocean Basins*, edited by A. D. Saunders and M. Norry, *Geol. Soc. Spec. Publ.*, *42*, 231–255.

deMenocal, P., J. Ortiz, T. Guilderson, J. Adkins, M. Sarnthein, L. Baker, and M. Yarusinsky (2000a), Abrupt onset and termination of the African Humid Period: Rapid climate responses to gradual insolation forcing, *Quat. Sci. Rev.*, *19*, 347–361, doi:10.1016/S0277-3791(99)00081-5.

deMenocal, P., et al. (2000b), Coherent high- and low-latitude climate variability during the Holocene Warm Period, *Science*, *288*, 2198–2202, doi:10.1126/science.288.5474.2198.

Derry, L. A., and C. France-Lanord (1996), Neogene Himalayan weathering history and river $^{87}Sr/^{86}Sr$: Impact on the marine Sr record, *Earth Planet. Sci. Lett.*, *142*(1–2), 59–74, doi:10.1016/0012-821X(96)00091-X.

Ennih, N., and J.-P. Liegeois (2008), The boundaries of the West African craton, with special reference to the basement of the Moroccan metacratonic Anti-Atlas belt, in *The Boundaries of the West African Craton*, edited by N. Ennih and J.-P. Liégeois, *Geol. Soc. Spec. Publ.*, *297*, 1–17.

Fagel, N., et al. (2002), Sources of Labrador Sea sediments since the last glacial maximum inferred from Nd-Pb isotopes, *Geochim. Cosmochim. Acta*, *66*(14), 2569–2581, doi:10.1016/S0016-7037(02)00866-9.

Faure, G. (1986), *Principles of Isotope Geology*, 589 pp., Wiley, New York.

Feng, J.-L., et al. (2011), Variations in trace element (including rare earth element) concentrations with grain sizes in loess and their implications for tracing the provenance of eolian deposits, *Quat. Int.*, doi:10.1016/j.quaint.2010.04.024, in press.

Gac, J. Y., and A. Kane (1986), Le fleuve Senegal: I. Bilan hydrologique et flux continentaux de matieres particulaires a l'embouchure, *Sci. Geol. Bull.*, *39*, 99–130.

Gasse, F., and E. van Campo (1994), Abrupt post-glacial climate events in West Asia and North Africa monsoon domains, *Earth Planet. Sci. Lett.*, *126*(4), 435–456.

Gasse, F., R. Téhet, A. Durand, E. Gibert, and J.-C. Fontes (1990), The arid–humid transition in the Sahara and the Sahel during the last deglaciation, *Nature*, *346*(6280), 141–146, doi:10.1038/346141a0.

Glaccum, R. A., and J. M. Prospero (1980), Saharan aerosols over the tropical North Atlantic—Mineralogy, *Mar. Geol.*, *37*(3–4), 295–321, doi:10.1016/0025-3227(80)90107-3.

Goldstein, S. L., and R. K. O'Nions (1981), Nd and Sr isotopic relationships in pelagic clays and ferromanganese deposits, *Nature*, *292*(5821), 324–327, doi:10.1038/292324a0.

Goldstein, S. L., et al. (1984), A Sm-Nd isotopic study of atmospheric dusts and particulates from major river systems, *Earth Planet. Sci. Lett.*, *70*(2), 221–236, doi:10.1016/0012-821X(84)90007-4.

Grousset, F. E., et al. (1998), Saharan wind regimes traced by the Sr-Nd isotopic composition of subtropical Atlantic sediments: Last glacial maximum vs today, *Quat. Sci. Rev.*, *17*, 395–409, doi:10.1016/S0277-3791(97)00048-6.

Holz, C., et al. (2004), Terrigenous sedimentation processes along the continental margin off NW-Africa: Implications from grain-size analyses of surface sediments, *Sedimentology*, *51*(5), 1145–1154, doi:10.1111/j.1365-3091.2004.00665.x.

Holz, C., et al. (2007), Variability in terrigenous sedimentation processes off northwest Africa and its relation to climate changes: Inferences from grain-size distributions of a Holocene marine sediment record, *Sediment. Geol.*, *202*(3), 499–508, doi:10.1016/j.sedgeo.2007.03.015.

Hooghiemstra, H. (1988), Changes of major wind belts and vegetation zones in NW Africa 20,000–5000 yr B.P., as deduced from a marine pollen record near cap blanc, *Rev. Palaeobot. Palynol.*, *55*(1–3), 101–140, doi:10.1016/0034-6667(88)90056-5.

Jacobsen, S. B., and G. J. Wasserburg (1980), Sm-Nd isotopic evolution of chondrites, *Earth Planet. Sci. Lett.*, *50*(1), 139–155, doi:10.1016/0012-821X(80)90125-9.

Jullien, E., et al. (2007), Low-latitude "dusty events" vs. high-latitude "icy Heinrich events", *Quat. Res.*, *68*(3), 379–386, doi:10.1016/j.yqres.2007.07.007.

Jung, S. J. A., et al. (2004), Stepwise Holocene aridification in NE Africa deduced from dust-borne radiogenic isotope records, *Earth Planet. Sci. Lett.*, *221*(1–4), 27–37, doi:10.1016/S0012-821X(04)00095-0.

Kennett, J. P. (1990), The Younger Dryas cooling event: An introduction, *Paleoceanography*, *5*(6), 891–895, doi:10.1029/PA005i006p00891.

Kutzbach, J. E., and F. A. Street-Perrott (1985), Milankovitch forcing of fluctuations in the level of tropical lakes from 18 to 0 kyr BP, *Nature*, *317*(6033), 130–134, doi:10.1038/317130a0.

Lecorche, J. P., et al. (1991), The Mauritanide orogeny and its northern extensions (Western Sahara and Zemmour), West Africa, in *The West African Orogens and Circum-Atlantic Correlatives*, edited by R. D. Dallmeyer and J. P. Lecorche, pp. 187–229, Springer, Berlin.

Liu, Z., et al. (2007), Simulating the transient evolution and abrupt change of Northern Africa atmosphere-ocean-terrestrial ecosystem in the Holocene, *Quat. Sci. Rev.*, *26*, 1818–1837, doi:10.1016/j.quascirev.2007.03.002.

Marret, F., and J.-L. Turon (1994), Paleohydrology and paleoclimatology off Northwest Africa during the last glacial-interglacial transition and the Holocene: Palynological evidences, *Mar. Geol.*, *118*(1–2), 107–117, doi:10.1016/0025-3227(94)90115-5.

McDermott, F., and C. J. Hawkesworth (1990), Intracrustal recycling and upper-crustal evolution: A case study from the Pan-African Damara mobile belt, central Namibia, *Chem. Geol.*, *83*(3–4), 263–280, doi:10.1016/0009-2541(90)90284-E.

Mulitza, S., M. Prange, J.-B. Stuut, M. Zabel, T. von Dobeneck, A. C. Itambi, J. Nizou, M. Schulz, and G. Wefer (2008), Sahel megadroughts triggered by glacial slowdowns of Atlantic meridional overturning, *Paleoceanography*, *23*, PA4206, doi:10.1029/2008PA001637.

Nicholson, S. E. (2000), The nature of rainfall variability over Africa on time scales of decades to millennia, *Global Planet. Change*, *26*, 137–158, doi:10.1016/S0921-8181(00)00040-0.

Nicholson, S. E., et al. (1980), African environmental and climatic changes and the general atmospheric circulation in late pleistocene and holocene, *Clim. Change*, *2*(4), 313–348, doi:10.1007/BF00137203.

Potrel, A., et al. (1996), 3.5 Ga old terranes in the West African Craton, Mauritania, *J. Geol. Soc.*, *153*(4), 507–510, doi:10.1144/gsjgs.153.4.0507.

Pye, K. (1987), *Aeolian Dust and Dust Deposits*, 334 pp., Academic, London.

Renssen, H., et al. (2006), Simulation of the Holocene climate evolution in Northern Africa: The termination of the African Humid Period, *Quat. Int.*, *150*, 95–102, doi:10.1016/j.quaint.2005.01.001.

Sarnthein, M., et al. (1982), Atmospheric and oceanic circulation patterns off northwest Africa during the past 25 million years, in *Geology of the Northwest African Continental Margin*, edited by U. Von Rad et al., pp. 545–604, Springer, Berlin.

Stuut, J.-B. W., et al. (2002), A 300-kyr record of aridity and wind strength in southwestern Africa: Inferences from grain-size distributions of sediments on Walvis Ridge, SE Atlantic, *Mar. Geol.*, *180*(1–4), 221–233, doi:10.1016/S0025-3227(01)00215-8.

Stuut, J.-B. W., M. Zabel, V. Ratmeyer, P. Helmke, E. Schefuß, G. Lavik, and R. Schneider (2005), Provenance of present-day eolian dust collected off NW Africa, *J. Geophys. Res.*, *110*, D04202, doi:10.1029/2004JD005161.

Tjallingii, R., et al. (2008), Coherent high- and low-latitude control of the northwest African hydrological balance, *Nat. Geosci.*, *1*(10), 670–675, doi:10.1038/ngeo289.

Trauth, M. H., and T. Schlüter (2006), *Geological Atlas of Africa: With Notes on Stratigraphy, Tectonics, Economic Geology, Geohazards and Geosites of Each Country*, 272 pp., Springer, Berlin.

Weldeab, S., et al. (2002), Provenance of lithogenic surface sediments and pathways of riverine suspended matter in the Eastern Mediterranean Sea: Evidence from $^{143}Nd/^{144}Nd$ and $^{87}Sr/^{86}Sr$ ratios, *Chem. Geol.*, *186*(1–2), 139–149, doi:10.1016/S0009-2541(01)00415-6.

Weltje, G. J., and M. A. Prins (2003), Muddled or mixed? Inferring palaeoclimate from size distributions of deep-sea clastics, *Sediment. Geol.*, *162*(1–2), 39–62, doi:10.1016/S0037-0738(03)00235-5.

Weltje, G. J., and M. A. Prins (2007), Genetically meaningful decomposition of grain-size distributions, *Sediment. Geol.*, *202*(3), 409–424, doi:10.1016/j.sedgeo.2007.03.007.

White, W. M., et al. (1986), Hf isotope ratios of marine sediments and Mn nodules: Evidence for a mantle source of Hf in seawater, *Earth Planet. Sci. Lett.*, *79*(1–2), 46–54, doi:10.1016/0012-821X(86)90039-7.

Wright, J. B., et al. (1985), *Geology and Mineral Resources of West Africa*, Allen and Unwin, London.